A Robust Cooperative Distributed Secondary Control Strategy for DC Microgrids With Fewer Communication Requirements

Mahdieh S. Sadabadi, *Senior Member, IEEE*, Nenad Mijatovic, *Senior Member, IEEE*, and Tomislav Dragičević, *Senior Member, IEEE*

***Abstract*—This article proposes a robust cooperative distributed secondary control strategy for dc microgrids, with the main focus on reducing communication burdens. To this end, we adopt a sparsity-promoting consensus-based distributed secondary control framework for converter-interfaced dc microgrids consisting of multiple distributed generation (DG) units. The proposed control strategy relies on less (sparse) information exchange over a communication network and does not require exchanging voltage signals or their estimated values amongst neighboring DG units. Rigorous Lyapunov-based stability certificates for dc microgrids are derived. The stability conditions can be verified without the knowledge of distribution lines connecting different DG units. The effectiveness of the proposed secondary control approach is verified by experimental results and a comparative simulation case study on a multiple-DG dc microgrid.**

***Index Terms*—DC microgrids, distributed control, distributed generation (DG), secondary control, stability analysis.**

I. Introduction

A. Motivation and Related Work

The paradigm shift from a centralized to a distributed secondary control system in dc microgrids has brought several advantages, such as improved scalability, enhanced reliability, and the resilience to a single point of failure [1], [2].

Cooperative and consensus-based distributed control algorithms have recently gained increasing attention for secondary control in dc microgrids, e.g., [3], [4], [5], [6], [7], [8], [9], [10], [11], and the references therein. The core idea in these approaches is based on information exchange and peer-to-peer communication amongst neighboring distributed generation (DG) units. For instance, distributed cooperative voltage and current control strategies in [3] and [9] require exchanging current and voltage signals of DG units, as well as the estimate of global average voltage values of dc–dc converters amongst their neighbors in order to achieve voltage balancing and proportional current sharing in dc microgrids. Despite several advantages that the consensus-based distributed secondary control strategies offer, they rely on communication and information exchanges in dc microgrids' control systems. Nevertheless, increasing the number of communication links and exchanged data brings several disadvantages due to communication delays, packet drop, and vulnerability to cyber-attacks, which adversely impact the reliability and resilience of dc microgrids. To decrease the communication burden in the secondary control of dc microgrids, event-triggered control mechanisms have recently been developed, e.g., [8], [12], [13], [14], in which continuous communication is not required. While the use of event-triggered distributed secondary control systems in dc microgrids has been growing, work related to the design of consensus protocols with less communication data has not fully been investigated. As distributed control strategies have been integrated into dc microgrids, the development of a sparse distributed control technique with fewer communication requirements that enhances the reliability and resilience of dc microrgids becomes crucial.

B. Statement of Contributions

Motivated by the abovementioned discussion, this article focuses on reducing the communication burden in the secondary control of dc microgrids from a different angle than an event-triggered control mechanism. The proposed nondroop-based distributed control strategy in this article reduces the communication burden in dc microgrids through two ways.

1) Unlike [3], [9], [12], and [13], the proposed secondary controller does not require exchanging voltage signals at the point of common couplings (PCCs) or estimated voltage signals among neighboring DG units.
2) Proposed secondary control approach in this article relies on less exchanged data, potentially resulting in a more reliable and resilient control solution for dc microgrids.

The proposed nondroop-based distributed secondary controller simultaneously guarantees voltage balancing and accurate proportional current-sharing amongst DG units and also guarantees the rigorous robust stability of dc microgrids (see Theorem 1). Detailed experimental and simulation results

Manuscript received 21 March 2022; revised 17 July 2022; accepted 19 August 2022. Date of publication 29 August 2022; date of current version 10 October 2022. Recommended for publication by Associate Editor J. Liu. *(Corresponding author: Mahdieh S. Sadabadi.)*

Mahdieh S. Sadabadi is with the School of Electronic Engineering and Computer Science, Queen Mary University of London, E1 4NS London, U.K. (e-mail: m.sadabadi@qmul.ac.uk).

Nenad Mijatovic and Tomislav Dragičević are with the Department of Electrical Engineering, Technical University of Denmark, 2800 Kongens Lyngby, Denmark (e-mail: nm@elektro.dtu.dk; tomdr@elektro.dtu.dk).

Color versions of one or more figures in this article are available at https://doi.org/10.1109/TPEL.2022.3202655.

Digital Object Identifier 10.1109/TPEL.2022.3202655

validate the performance of the proposed distributed controller in terms of robust performance under load changes and distribution line failure. Furthermore, comparative case studies with recent secondary control protocols highlight that while the proposed control strategy relies on fewer information exchanges, it provides satisfactory performance in the voltage and current trajectories of DG units.

The rest of this article is organized as follows. The dynamical model of a converter-interfaced dc microgrid is presented in Section II. A novel consensus-based distributed secondary control for achieving voltage balancing and current sharing in dc microgrids is developed in Section III and analyzed in Section IV. Section V is devoted to simulation and experimental results. Finally, Section VI concludes this article.

C. Notations and Preliminaries

Notations: The notations used in this article are standard. In particular, matrix $\mathbf{I}_n$ is an $n \times n$ identity matrix and $\mathbf{1}_n$ is an n-dimensional vector of all ones. The symbols A^T, rank(A), ker(A), det(A), trace(A), and diag$(a_1, \ldots, a_n)$, respectively, denote the transpose, rank, kernel (null space), determinant, and trace of A, and a diagonal matrix whose diagonal elements are a_i. For symmetric matrices, $P \succ 0$ ($P \prec 0$) and $P \succeq 0$ ($P \preceq 0$), respectively, indicate the positive definiteness (negative definiteness) and the positive semidefiniteness (negative semidefiniteness). Furthermore, for two symmetric matrices A and B, $A \succ B$ means that $A - B \succ 0$.

Preliminaries: An undirected graph $\mathcal{G} = (\mathcal{V}, \mathcal{E})$ is defined by a node (vertex) set $\mathcal{V} = \{1, .., n\}$ and an edge set $\mathcal{E} \subseteq \mathcal{V} \times \mathcal{V}$. The adjacency matrix of $\mathcal{G}$ is an $n \times n$ matrix $\mathbb{A} = [a_{ij}]$ whose elements are determined as $a_{ij} = 1$ if $(i, j) \in \mathcal{E}$; otherwise, $a_{ij} = 0$ [15]. The degree matrix $\mathbb{D} = [d_{ij}]$ is an $n \times n$ diagonal matrix whose diagonal elements $d_{ii} = \deg(v_i)$, where $\deg(v_i)$ of node i counts the number of times an edge terminates at that node. Given an undirected graph $\mathcal{G}$ with n nodes, m edges, adjacency matrix $\mathbb{A}$, and degree matrix $\mathbb{D}$, the Laplacian matrix of $\mathcal{G}$ is $\mathbb{L} = \mathbb{D} - \mathbb{A}$ [15]. Moreover, the (oriented) incidence matrix $\mathbb{B} = [b_{ij}] \in \mathbb{R}^{n \times m}$ of the graph $\mathcal{G}$ is defined componentwise as follows [15]:

$$b_{ij} = \begin{cases} 1 & \text{if node } \ i \ \text{ is the source node of edge } \ j \\ -1 & \text{if node } \ i \ \text{ is the sink node of edge } \ j \\ 0 & \text{otherwise.} \end{cases} \tag{1}$$

II. Dynamical Model of DC Microgrids

Consider a converter-interfaced dc microgrid composed of n DG units. Renewable energy sources connected via dc–dc converters are interconnected to each other via m resistive–inductive distribution lines. Fig. 1 shows the schematic diagram of a converter-interfaced DG i and DG j connecting via a resistive-inductive distribution line k.

A. Dynamics of Converter-Interfaced DG Units

Using the electric circuit theory, the dynamics of converter-interfaced DG unit i are described as follows:

$$C_{t_i}\dot{V}_i(t) = I_{t_i}(t) - Y_i V_i(t) - \sum_{k=1}^{m} \mathbb{B}_{e,ik} I_k(t)$$

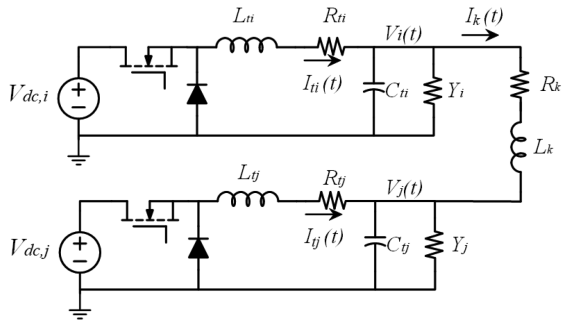

Fig. 1. Schematic diagram of a converter-interfaced DG i and DG j connecting via a resistive–inductive distribution line k.

$$\begin{aligned} L_{t_i}\dot{I}_{t_i}(t) &= -V_i(t) - R_{t_i} I_{t_i}(t) + V_{\mathrm{dc},i} d_i(t) \\ L_k \dot{I}_k(t) &= -R_k I_k(t) + \sum_{j=1}^{n} \mathbb{B}_{e,jk} V_j(t) \end{aligned} \tag{2}$$

for $i \in \{1, \ldots, n\}$ and $k \in \{1, \ldots, m\}$, where L_{t_i}, R_{t_i}, C_{t_i}, Y_i, (R_k, L_k), and $V_{\mathrm{dc},i}$ represent the filter inductance of the converter i, the parasitic resistance of the inductance L_{t_i}, a shunt capacitance, load conductance, the resistance and inductance of the distribution line k, and the dc voltage at the input side of the converter i, respectively. In (2), $V_i(t) \in \mathbb{R}$, $I_{t_i}(t) \in \mathbb{R}$, $d_i(t) \in \mathbb{R}$, and $I_k(t) \in \mathbb{R}$ are the voltage at the PCC i, the filter current, the duty cycle of the dc–dc converter i, and the current of line k, respectively. The control input in (2) is defined as $u_i(t) = V_{\mathrm{dc},i} d_i(t)$. The direction of the distribution line current is arbitrary chosen, and the term $\mathbb{B}_{e,ik}$ is formulated as follows [16]:

$$\mathbb{B}_{e,ik} = \begin{cases} 1 & \text{if line } \ k \ \text{ leaves DG } \ i \\ -1 & \text{if line } \ k \ \text{ enters DG } \ i \\ 0 & \text{otherwise.} \end{cases} \tag{3}$$

Assumption 1: It is assumed that loads are connected at the PCC of each DG unit.

Assumption 1 is reasonable as it has been shown that the general interconnection of loads and DG units can always be mapped into this structure using a Kron reduction method [17].

The dc microgrid in (2) forms a network represented by an undirected connected graph $\mathcal{G}_e = (\mathcal{V}, \mathcal{E})$, where $\mathcal{V}$ and $\mathcal{E}$ are the sets of vertices and edges, respectively. Each element in the vertex set $\mathcal{V} = \{1, .., n\}$ represents a DG unit and each element in the edge set $\mathcal{E} = \{1, .., m\}$ represents a distribution line connecting different DG units.

Let $V(t) = [V_1(t) \ \ldots \ V_n(t)]^T$, $I_t(t) = [I_{t_1}(t) \ \ldots \ I_{t_n}(t)]^T$, $I(t) = [I_1(t) \ \ldots \ I_m(t)]^T$, and $u(t) = [u_1(t) \ \ldots \ u_n(t)]^T$. The dc microgrid is then mathematically described in a vector form by the following :

$$\begin{aligned} [C_t]\,\dot{V}(t) &= I_t(t) - \mathbb{B}_e I(t) - [Y]\,V(t) \\ [L_t]\,\dot{I}_t(t) &= -V(t) - [R_t]\,I_t(t) + u(t) \\ [L]\,\dot{I}(t) &= \mathbb{B}_e^T V(t) - [R]\,I(t) \end{aligned} \tag{4}$$

where $[C_t] = \mathrm{diag}(C_{t_1}, \ldots, C_{t_n})$, $[L_t] = \mathrm{diag}(L_{t_1}, \ldots, L_{t_n})$, $[R_t] = \mathrm{diag}(R_{t_1}, \ldots, R_{t_n})$, $[L] = \mathrm{diag}(L_1, \ldots, L_m)$, and $[R] = \mathrm{diag}(R_1, \ldots, R_m)$.

The microgrid topology is described by an (oriented) incidence matrix $\mathbb{B}_e \in \mathbb{R}^{n\times m}$ of the undirected graph $\mathcal{G}_e$, whose ik element is $\mathbb{B}_{e,ik}$ in (3). The Laplacian matrix associated with the graph $\mathcal{G}_e$ is represented by $\mathbb{L}_e = \mathbb{B}_e[R]^{-1}\mathbb{B}_e^T$.

B. Current Sharing and Voltage Balancing Requirements in DC Microgrids

In the secondary control of dc microgrids, one of the main control objectives is to proportionally share the total load demands amongst DG units at the steady-state according to the rated currents of DG units, i.e.,

$$\lim_{t\to\infty}\left(\frac{I_{t_i}(t)}{I_i^{\text{rated}}}-\frac{I_{t_j}(t)}{I_j^{\text{rated}}}\right)=0,\quad i,j\in\{1,\ldots,n\} \tag{5}$$

where $I_{t_i}(t)$, $I_{t_j}(t)$, I_i^{rated}, and I_j^{rated} are the current of the converter i and converter j, the rated current of converter i, and the rated current of converter j, respectively. As one can observe from (5), achieving the proportional current sharing is equivalent to a consensus on $I_i^{\text{rated}^{-1}} I_{t_i}(t)$.

The second secondary control objective in dc microgrids is voltage regulation at PCCs to a given reference value V^* at the steady state, i.e., $\lim_{t\to\infty} V_i(t) = V^*$. However, the requirement of current sharing in (5) does not allow such a voltage regulation. As a reasonable alternative, the weighted average value of voltage signals at PCCs is regulated at the weighted average value of V^* at the steady state. The weights can usually be chosen to be equal to the rated current of converters, as this implies a relatively small voltage deviation from V^* for dc–dc converters with a relatively large generation capacity [18]. The voltage balancing objective is mathematically formulated as follows:

$$\lim_{t\to\infty}\frac{1}{n}\sum_{i=1}^{n} I_i^{\text{rated}}(V_i(t)-V^*)=0. \tag{6}$$

It should be noted that the voltage reference V^* in (6) is generated by an upper-level control, referred to as the tertiary control [7]. The tertiary controller sends the reference value of V^* to the secondary control layer. As a result, the value of V^* is known for the secondary controller in dc microgrids.

In case all dc–dc converters have equal generation capacities, the following equal current sharing and average voltage regulation objectives can be considered—this can be considered as a special case of (5) and (6):

$$\begin{aligned}&\lim_{t\to\infty}\big(I_{t_i}(t)-I_{t_j}(t)\big)=0,\quad i,j\in\{1,\ldots,n\}\\ &\lim_{t\to\infty}\frac{1}{n}\sum_{i=1}^{n}(V_i(t)-V^*)=0.\end{aligned} \tag{7}$$

C. Communication Requirements in DC Microgrids' Secondary Control

To address proportional current sharing and voltage balancing requirements in (5) and (6), the common secondary control strategy in dc microgrids is based on cooperative and distributed control mechanisms. In this secondary control setting, each DG units exchanges its current $I_{t_i}(t)$, its local PCC voltage $V_i(t)$, and the estimated value of the average voltage across the microgrid $\hat{V}_i(t)$ with its neighboring DG units on a communication graph with an adjacency matrix $\mathbb{A}=[a_{ij}]\in\mathbb{R}^{n\times n}$ and a Laplacian matrix $\mathbb{L}\in\mathbb{R}^{n\times n}$. For instance, the cooperative secondary controller in [9] at converter i, based on the relative information with respect to neighboring DG units, relies on the following control law:

$$\begin{aligned}u_{n_i}(t)&=c_i\left(\gamma_i(V^*-\hat{V}_i(t))+\sum_{j\in\mathcal{N}_i}a_{ij}\left(\frac{I_{t_j}(t)}{I_j^{\text{rated}}}-\frac{I_{t_i}(t)}{I_i^{\text{rated}}}\right)\right)\\ \dot{\hat{V}}_i(t)&=\dot{V}_i(t)+c_i\sum_{j\in\mathcal{N}_i}a_{ij}(\hat{V}_j(t)-\hat{V}_i(t))\end{aligned} \tag{8}$$

where $c_i\in\mathbb{R}_{>0}$ is a coupling gain, $\mathcal{N}_i$ is the set of neighbors of DG i, and c_i and γ_i are design parameters. The secondary controller in (8) sends a set-point $V_{n_i}=\int u_{n_i}(t)dt$ to a primary control level operating based on a droop mechanism.

The cooperative secondary control in (8) requires exchanging the current and the estimated voltage of DG units amongst neighboring DG units according to the adjacency matrix $\mathbb{A}$. While the consensus-based secondary control strategy in (8) guarantees (5) and (6), it relies on the excess of communication and information exchanges in dc microgrid control systems. Therefore, in order to enhance the reliability and resilience of dc microgrids, it is essential to develop a sparse consensus-based secondary control algorithm that ensures achieving the current sharing and voltage balancing requirements. Motivated by this challenging issue, in this article, a novel consensus-based secondary control algorithm is developed that relies on limited information exchanges amongst neighboring DG units.

III. Proposed Distributed Secondary Control in DC Microgrids

This section proposes a novel consensus-based distributed secondary control strategy to address voltage balancing and current-sharing problems in dc microgrids. The developed secondary controllers communicate through a distributed sparse communication layer, which shares information only amongst the neighboring DG units.

A. Consensus-Based Distributed Secondary Control Approach

The main objective of this article is to design a consensus-based secondary control strategy that utilizes fewer communication links compared with the existing cooperative distributed secondary controllers, e.g., the proposed distributed control law in (8).

The proposed consensus-based controller in this article combines both secondary and primary control levels in dc microgrids. As a result, the outputs of the controller are directly sent to the duty cycles of dc–dc converters without relying on a droop control mechanism.

The proposed distributed controller introduces three layers where there are cross-layer interactions amongst them. The communication network of the proposed distributed control approach is based on an unweighted undirected communication graph $\mathcal{G}$ of n nodes and k edges, where $k\geq n-1$.

The upper layer of the proposed secondary controller that is responsible for the proportional current sharing objective in (5) is presented as follows:

$$\tau_v \dot{v}(t) = -K\mathbb{B}^T W^{-1} I_t(t) \tag{9}$$

where $K > 0$, $\tau_v > 0$, and $W = \text{diag}(I_1^{\text{rated}}, \ldots, I_n^{\text{rated}})$, $\mathbb{B}$ is the (oriented) incidence matrix of the graph $\mathcal{G}$, and $v(t)$ is a state vector of the proposed controller. The abovementioned dynamics ensure the proportional current sharing as it involves the incidence matrix $\mathbb{B}$ in the feedback loop of $I_t(t)$. Note that at the steady state, it follows that steady-state (proportional) current sharing is achieved as all the elements of $W^{-1}\bar{I}_t$ are identical ($\bar{I}_t$ is the steady-state value of the current vector $I_t(t)$).

The middle layer of the proposed secondary controller is described as follows:

$$\begin{aligned} \tau_\phi \dot{\phi}(t) &= -\beta(V(t) - \mathbf{1}_n V^*) + z(t) \\ \tau_\theta \dot{\theta}(t) &= I_t(t) - \theta(t) \\ z(t) &= K_P(\theta(t) - I_t(t)) + KW^{-1}\mathbb{B}v(t) \end{aligned} \tag{10}$$

where $\beta > 0$, $K_P > 0$, $\tau_\phi > 0$, and $\tau_\theta > 0$. In (10), $\phi(t)$ and $\theta(t)$ are two state vectors of the proposed controller.

The middle layer ensures the voltage balancing objective in (6). Note that the additional term $K_P(\theta(t) - I_t(t))$ in (10) does not alter the steady-state conditions, i.e., the voltage balancing/current sharing; however, this term improves the dynamics responses of DG units by preventing the occurrence of oscillations.

Next, the control law of the lower layer of the proposed distributed controller is given as follows:

$$u(t) = K_1 V(t) + K_2 I_t(t) + K_3 \phi(t) + (1 - K_1)\beta^{-1} z(t) \tag{11}$$

where K_1, K_2, and K_3 are the design parameters that are designed to guarantee the closed-loop stability. Finally, $d_i(t) = \frac{1}{V_{dc,i}} u_i(t)$ is applied to the duty cycles of dc–dc converters.

In the abovementioned distributed control scheme over the undirected communication graph $\mathcal{G}$, the topology of $\mathcal{G}$ can generally be different from the topology of the microgrid electrical graph $\mathcal{G}_e$. The following assumption is made on the underlying communication graph of the proposed distributed controller.

Assumption 2: It is assumed that the topology of the communication undirected graph $\mathcal{G}$ is connected.

B. Communication Requirements

As one can observe from the dynamics of the multilayer controller in (9)–(11), as follows:

1) the proposed control scheme does not rely on exchanging voltage signals $V_i(t)$ and voltage estimates $\hat{V}_i(t)$ amongst neighboring DG units;
2) the knowledge of the microgrid topology, line impedances, and loads is not required; and
3) the proposed control framework in (9)–(11) requires fewer communication exchanges to achieve the current-sharing and average voltage regulation objectives in (5) and (6).

For more clarity on the communication burdens of the proposed consensus-based control technique in terms of the number of information exchanges, the following example is given to highlight the superiority of (9)–(11) over the existing cooperative secondary control approaches in dc microgrids.

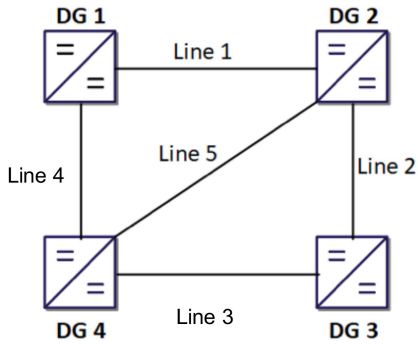

Fig. 2. Schematic diagram of the physical layer of a dc Microgrid with $n = 4$ DG units connecting via $m = 5$ lines in Example 1.

Example 1: Consider a dc microgrid consisting of $n = 4$ DG units connecting via $m = 5$ distribution lines, as graphically shown in Fig. 2. It is assumed that the underlying communication network in the consensus-based control layer of the microgrid is based on the following adjacency matrix $\mathbb{A} \in \mathbb{R}^{4\times 4}$ and its corresponding oriented incidence matrix $\mathbb{B} \in \mathbb{R}^{4\times 5}$:

$$\mathbb{A} = \begin{bmatrix} 0 & 1 & 0 & 1 \\ 1 & 0 & 1 & 1 \\ 0 & 1 & 0 & 1 \\ 1 & 1 & 1 & 0 \end{bmatrix}, \quad \mathbb{B} = \begin{bmatrix} 1 & 0 & 0 & 1 & 0 \\ -1 & 1 & 0 & 0 & 1 \\ 0 & -1 & 1 & 0 & 0 \\ 0 & 0 & -1 & -1 & -1 \end{bmatrix}. \tag{12}$$

According to (8), $x_2(t) = [\hat{V}_2(t), \frac{I_{t_2}(t)}{I_2^{\text{rated}}}]$ and $x_4(t) = [\hat{V}_4(t), \frac{I_{t_4}(t)}{I_4^{\text{rated}}}]$ are transmitted to the controller of converter 1, $x_1(t) = [\hat{V}_1(t), \frac{I_{t_1}(t)}{I_1^{\text{rated}}}]$, $x_3(t) = [\hat{V}_3(t), \frac{I_{t_3}(t)}{I_3^{\text{rated}}}]$, and $x_4(t) = [\hat{V}_4(t), \frac{I_{t_4}(t)}{I_4^{\text{rated}}}]$ are sent to the controller of converter 2, $x_2(t) = [\hat{V}_2(t), \frac{I_{t_2}(t)}{I_2^{\text{rated}}}]$ and $x_4(t) = [\hat{V}_4(t), \frac{I_{t_4}(t)}{I_4^{\text{rated}}}]$ are transmitted to the controller of converter 3, and $x_1(t) = [\hat{V}_1(t), \frac{I_{t_1}(t)}{I_1^{\text{rated}}}]$, $x_2(t) = [\hat{V}_2(t), \frac{I_{t_2}(t)}{I_2^{\text{rated}}}]$, and $x_3(t) = [\hat{V}_3(t), \frac{I_{t_3}(t)}{I_3^{\text{rated}}}]$ are transmitted to the controller of converter 4.

Based on the proposed consensus algorithm in (9)–(11), $\frac{I_{t_2}(t)}{I_2^{\text{rated}}}$, $v_1(t)$, and $v_4(t)$ are transmitted to the controller of converter 1, $\frac{I_{t_3}(t)}{I_3^{\text{rated}}}$, $v_1(t)$, $v_2(t)$, and $v_5(t)$ are sent to the local controller of converter 2, $\frac{I_{t_4}(t)}{I_4^{\text{rated}}}$, $v_2(t)$, and $v_3(t)$ are transmitted to the local controller of converter 3, and $\frac{I_{t_1}(t)}{I_1^{\text{rated}}}$, $v_3(t)$, $v_4(t)$, and $v_5(t)$ are transmitted to the controller of converter 4.

This example shows that although both conventional and proposed secondary controllers rely on the same communication graph, [$\mathbb{A}$ and $\mathbb{B}$ in (12) are the same for both control approaches] the proposed distributed control strategy in (9)–(11) requires fewer data exchanges over a communication network than the proposed distributed controller in [9] [distributed secondary control in (8)]. Furthermore, Lemma 1 in Section IV shows that the use of the incidence matrix $\mathbb{B}$ in (9)–(11) instead of the Laplacian matrix does not affect the current-sharing consensus

and voltage balancing objectives. Note that the underlying communication graph in both conventional and proposed secondary control strategies is the same; however, the proposed secondary control method relies on less exchanged data. Moreover, the communication graph in the secondary control layer can be chosen to be the same as the communication graph in the physical layer of dc microgrids. It means that if two DG units are physically connected via a power line, they can transmit their current and/or control states to each other (a neighbor-to-neighbor communication scheme).

Remark 1: In terms of the communication graph, the underlying graph in the proposed secondary controller is assumed to undirected. However, information exchange amongst DG units' controllers is not necessarily bidirectional. For instance, in Example 1, $\frac{I_{t_2}(t)}{I_2^{\text{rated}}}$ is sent to the controller of DG 1 while $\frac{I_{t_1}(t)}{I_1^{\text{rated}}}$ is not transmitted to the controller of DG 2; instead, $v_2(t)$ is sent.

Remark 2: The proposed secondary control scheme in (9)–(11) is robust with respect to line failures as long as the underlying communication graph remains connected.

C. Closed-Loop Dynamics

The Overall dc microgrid with the distributed control in (9)–(11) is presented as follows:

$$
\begin{aligned}
&[L_t]\,\dot{I}_t(t) = (-1+K_1)V(t) + (K_2\mathbf{I}_n - [R_t])I_t(t) + K_3\phi(t)\\
&\quad\times(1-K_1)\left(\frac{K_P}{\beta}W(\theta(t)-I_t(t)) + \frac{K}{\beta}W^{-1}\mathbb{B}v(t)\right)\\
&\tau_\phi\dot{\phi}(t) = -\beta(V(t)-\mathbf{1}_nV^*) + K_P(\theta(t)-I_t(t)) + KW^{-1}\mathbb{B}v(t)\\
&\tau_v\dot{v}(t) = -K\mathbb{B}^TW^{-1}I_t(t)\\
&\tau_\theta\dot{\theta}(t) = I_t(t)-\theta(t)\\
&[C_t]\,\dot{V}(t) = I_t(t) - \mathbb{B}_eI(t) - [Y]\,V(t)\\
&[L]\,\dot{I}(t) = \mathbb{B}_e^TV(t) - [R]\,I(t)
\end{aligned}
\tag{13}
$$

where $W=\text{diag}(I_1^{\text{rated}},\ldots,I_n^{\text{rated}})$, $v(t)=[v_1\ \ \ldots\ \ v_k]^T$, $\theta(t)=[\theta_1\ \ \ldots\ \ \theta_n]^T$, $\phi(t)=[\phi_1\ \ \ldots\ \ \phi_n]^T$, $K_P=\text{diag}(K_{P_1},\ldots,K_{P_n})$, and $K_j=\text{diag}(K_{j,1},\ldots,K_{j,n})$, $j=1,2,3$.

Remark 3: (Comment on the trajectories of $v(t)$) Let Assumption 2 hold. For any $K>0$ and $\tau_v>0$, the trajectory $v(t)$ in (13) starting from any initial condition $v(0)$ satisfies the following condition:

$$y^Tv(t) = y^Tv(0)\quad\forall t\geq 0 \tag{14}$$

where $y\in ker(\mathbb{B})$ [10].

In the next section, the stability of the closed-loop dc microgrid in (13) will be analyzed. Moreover, it is shown that the proportional current sharing and voltage balancing in (5) and (6) are simultaneously guaranteed via (9)–(11).

IV. Stability Analysis

In this section, we discuss the existence of equilibria and analyze the stability of dc microgrids with the proposed consensus-based control mechanism in (9)–(11). The main results are given in Lemma 1 and Theorem 1, respectively.

A. Analysis of Equilibria

The following lemma discusses the existence of equilibria for the overall dc microgrid in (13).

Lemma 1: Consider the dynamics of the overall dc microgrid in (13) under a connected undirected communication graph. There exist equilibria $(\bar{V},\bar{I}_t,\bar{\theta},\bar{v},\bar{I},\bar{\phi})$ that are characterized as follows:

$$
\begin{aligned}
&\begin{bmatrix}\mathbb{L}_t+\mathbb{L}_e\\ \mathbf{1}_n^TW\end{bmatrix}\bar{V} = \begin{bmatrix}0\\ \mathbf{1}_n^TW\mathbf{1}_nV^*\end{bmatrix}\\
&\bar{I}_t = \frac{1}{\mathbf{1}_n^TW\mathbf{1}_n}W\mathbf{1}_n\mathbf{1}_n^T\,[Y]\,\bar{V}\\
&\bar{\theta} = \bar{I}_t\\
&\bar{v} = \begin{cases}\left(\frac{v_0^Tv(0)}{v_0^Tv_0}\right)v_0 + \beta K^{-1}\mathbb{B}^+W(\bar{V}-\mathbf{1}_nV^*) & \text{if } v_0\neq 0\\ \beta K^{-1}\mathbb{B}^+W(\bar{V}-\mathbf{1}_nV^*) & \text{if } v_0=0\end{cases}\\
&\bar{I} = [R]^{-1}\,\mathbb{B}_e^T\bar{V}\\
&\bar{\phi} = [K_3]^{-1}\\
&\quad\times\left((1-K_1)\bar{V} - (K_2\mathbf{I}_n-[R_t])\bar{I}_t - \frac{K}{\beta}(1-K_1)W^{-1}\mathbb{B}\bar{v}\right)
\end{aligned}
\tag{15}
$$

where $\mathbb{L}_t=(\mathbf{I}_n-(\mathbf{1}_n^TW\mathbf{1}_n)^{-1}W\mathbf{1}_n\mathbf{1}_n^T)[Y]$, $\mathbb{L}_e=\mathbb{B}_e[R]^{-1}\mathbb{B}_e^T$, $v_0\in ker(\mathbb{B})$, and $\mathbb{B}^+$ is the Moore–Penrose generalized inverse of the incidence matrix $\mathbb{B}$.

Proof: See Appendix B. □

Remark 4: Based on the rank–nullity theorem, the dimension of $ker(\mathbb{B})=k-n+1\geq 0$. Therefore, $\bar{v}$ might not be unique.

B. Stability Analysis

This section analyzes the stability of dc microgrids with the proposed control strategy in (9)–(11). The main results are presented in Theorem 1.

By change of variables as $e_V(t)=V(t)-\bar{V}$, $e_{I_t}(t)=I_t(t)-\bar{I}_t$, $e_\theta(t)=\theta(t)-\bar{\theta}$, $e_v(t)=v(t)-\bar{v}$, $e_\phi(t)=\phi(t)-\bar{\phi}$, and $e_I(t)=I(t)-\bar{I}$, the closed-loop dc microgrid augmented with the consensus control in (9)–(11) can be represented as follows:

$$
\begin{aligned}
&[L_t]\,\dot{e}_{I_t}(t) = (-1+K_1)e_V(t)\\
&\quad + (K_2\mathbf{I}_n-[R_t])e_{I_t}(t) + K_3e_\phi(t)\\
&\quad + (1-K_1)\left(\beta^{-1}K_PW(e_\theta(t)-e_{I_t}(t)) + \frac{K}{\beta}W^{-1}\mathbb{B}e_v(t)\right)\\
&\tau_\phi\dot{e}_\phi(t) = -\beta e_V(t) + K_P(e_\theta(t)-e_{I_t}(t)) + KW^{-1}\mathbb{B}e_v(t)\\
&\tau_v\dot{e}_v(t) = -K\mathbb{B}^TW^{-1}e_{I_t}(t)\\
&\tau_\theta\dot{e}_\theta(t) = e_{I_t}(t)-e_\theta(t)\\
&[C_t]\,\dot{e}_V(t) = e_{I_t}(t) - \mathbb{B}_ee_I(t) - [Y]\,e_V(t)\\
&[L]\,\dot{e}_I(t) = \mathbb{B}_e^Te_V(t) - [R]\,e_I(t).
\end{aligned}
\tag{16}
$$

Theorem 1: Let Assumption 2 hold. For any $\tau_v>0$, $\tau_\theta>0$, $\tau_\phi>0$, $\beta>0$, $K>0$, $K_P\succ 0$, $K_1\prec 1$, $K_2\prec R_{t_i}$, and $0\prec$

$K_3 \prec \frac{\tau_\theta}{\beta} L_{t_i}^{-1}(R_{t_i} - K_2)(1 - K_1)$, $i = 1, \ldots, n$, the following statements hold.

1) The origin in (16) is globally asymptotically stable.
2) The proportional current sharing and voltage balancing in (5) and (6) are guaranteed.

Proof: We propose the following quadratic-type Lyapunov function $\mathcal{V} \geq 0$ for dc microgrids whose dynamics are given in (16):

$$\mathcal{V} = \frac{\tau_\theta}{2\beta} e_\theta^T(t) K_P e_\theta(t) + \frac{\tau_v K}{2\beta} e_v^T(t) e_v(t) + \frac{1}{2} e_V^T(t) \left[C_t\right] e_V(t) + \frac{1}{2} e_I^T(t) \left[L\right] e_I(t) + \frac{1}{2} \sum_{i=1}^{n} \left[e_{I_{t_i}} \; e_{\phi_i} \right] P_i \left[e_{I_{t_i}} \; e_{\phi_i} \right]^T \tag{17}$$

where

$$P_i = \frac{\begin{bmatrix} L_{t_i}(R_{t_i} - K_2) & -L_{t_i} K_3 \\ -L_{t_i} K_3 & \frac{\tau_\phi}{\beta}(1 - K_1) K_3 \end{bmatrix}}{(R_{t_i} - K_2)(1 - K_1) - \frac{L_{t_i}\beta}{\tau_\phi} K_3}. \tag{18}$$

Since $P_i \in \mathbb{R}^{2\times 2}$, $\det(P_i) = \frac{\tau_\phi}{\beta} K_3 > 0$, and $\text{trace}(P_i) > 0$, $P_i \succ 0$.

In the next step, the time derivative of $\mathcal{V}$ along the closed-loop microgrid trajectories in (16) is obtained. It can be shown that $\dot{\mathcal{V}}$ can be obtained as follows:

$$\dot{\mathcal{V}} = -\frac{1}{\beta}(e_{I_t} - e_\theta)^T K_P (e_{I_t} - e_\theta) - e_I^T \left[R\right] e_I - e_V^T \left[Y\right] e_V + \frac{1}{2} \sum_{i=1}^{n} \left[e_{I_{t_i}} \; e_{\phi_i} \right] Q_i \left[e_{I_{t_i}} \; e_{\phi_i} \right]^T \tag{19}$$

where

$$Q_i = \frac{\begin{bmatrix} -2(R_{t_i} - K_2)^2 & \star \\ 2K_3(R_{t_i} - K_2) & -2K_{3,i}^2 \end{bmatrix}}{(R_{t_i} - K_2)(1 - K_1) - \frac{L_{t_i}\beta}{\tau_\phi} K_3}. \tag{20}$$

It can be shown that $\det(Q_i) = 0$ and $\text{trace}(Q_i) = -2(R_{t_i} - K_2)^2 - 2K_3^2 < 0$; hence, $Q_i \in \mathbb{R}^{2\times 2} \preceq 0$. As a result, $\dot{\mathcal{V}} \leq 0$.

In the next step, we will show that the origin in (16) is globally asymptotically stable. To this end, it is illustrated that the only solution of $\dot{\mathcal{V}} = 0$ is the origin for all $t \geq 0$ (LaSalle's invariance principle [19]). To see this, note that the state trajectories that make $\dot{\mathcal{V}} = 0$ belong to the following set:

$$\chi = \underbrace{\left\{e_I^T \left[R\right] e_I = 0\right\}}_{\chi_1} \cap \underbrace{\left\{e_V^T \left[Y\right] e_V = 0\right\}}_{\chi_2} \cap \underbrace{\left\{(e_{I_t} - e_\theta)^T K_P (e_{I_t} - e_\theta) = 0\right\}}_{\chi_3} \cap \underbrace{\left\{ \left[e_{I_{t_i}} \; e_{\phi_i} \right]^T \in \ker(Q_i),\; i = 1, \ldots, n \right\}}_{\chi_4}. \tag{21}$$

In the following, we show that that the only state trajectory $(\tilde{e}_{I_t}, \tilde{e}_V, \tilde{e}_I, \tilde{e}_v, \tilde{e}_\theta, \tilde{e}_\phi)$ of (16) in χ is the origin. The sets χ_1, χ_2, and χ_3, respectively, imply that $\tilde{e}_I = 0$, $\tilde{e}_V = 0$, and $\tilde{e}_{I_t} = \tilde{e}_\theta$. From the kernel Q_i in χ_4, one can obtains that $\tilde{e}_{I_{t_i}} = \frac{K_3}{R_{t_i} - K_2} \tilde{e}_{\phi_i}$, $i = 1, \ldots, n$. Hence, from the system dynamics in (16) and the set χ one obtains that $\tilde{e}_{I_t} = 0$; hence, $\tilde{e}_\phi = 0$ and $\tilde{e}_\theta = 0$, and $W^{-1}\mathbb{B}\tilde{e}_v = 0$. Therefore, $\tilde{e}_v$ belongs to the null space of $\mathbb{B}$, i.e., $\tilde{e}_v = \tilde{\beta} e_v^*$, where $\tilde{\beta} \in \mathbb{R}$ is a constant and $e_v^* \in \ker(\mathbb{B})$. By replacing $\tilde{e}_v$ by $v - \bar{v}$ we have $v - \bar{v} = \nu e_v^*$; hence, $(e_v^*)^T(v - \bar{v}) = \nu({e_v^*}^T e_v^*)$. According to (14), ${e_v^*}^T v = {e_v^*}^T \bar{v}$. As a result, $\nu = 0$ and $\tilde{e}_v = 0$. This implies that the largest invariant set of χ is the origin. Therefore, there are not any other trajectories in (16) that converge to the origin.

In the final step, it is shown that (9)–(11) guarantees the voltage balancing and current sharing objectives. Due to the asymptotic stability of the origin in (16), the voltage and current of the converters converge to the equilibria $\bar{V}$ and $\bar{I}_t$, respectively. According to Lemma 1, $\bar{V}$ and $\bar{I}_t$ are characterized as follows:

$$\bar{I}_t = \frac{1}{\mathbf{1}_n^T W \mathbf{1}_n} W \mathbf{1}_n \mathbf{1}_n^T \left[Y\right] \bar{V}$$
$$0 = \mathbf{1}_n^T W \left(\bar{V} - \mathbf{1}_n V^*\right). \tag{22}$$

By premultiplying the first equation in (22) by W^{-1}, one obtains that $W^{-1}\bar{I}_t$ is equal to a constant vector. Moreover, the second equation in (22) indicates that the average voltage regulation in (6) is ensured. □

Remark 5 [Comment on Robustness of (9)–(11) to uncertainties in physical parameters of DG microgrids]: According to the stability conditions proposed in Theorem 1, it can be shown that the robust stability as well as proportional current sharing and voltage regulation objectives are guaranteed regardless of load values and the parameters of distribution lines.

C. Distributed Control Design Algorithm

In this section, the results given in Theorem 1 are summarized and a design algorithm for the parameters of the proposed distributed control approach in (9)–(11) is introduced. As mentioned in Remark 5, the design of the controller parameters is independent of distribution lines and load parameters. The algorithm is summarized as follows.

Proposed algorithm for the design of consensus-based distributed controllers in dc microgrids:

1) *Distributed control structure:* The controller for each DG unit is structured by (9)–(11).
2) *Design of communication graph:* The communication graph in the control layer can be the same as the communication graph in the physical layer of dc microgrids.
3) *Design of control parameters in (9)–(11):* $\tau_v > 0$, $\tau_\theta > 0$, $\tau_\phi > 0$, $\beta > 0$, $K > 0$, $K_P > 0$, $K_1 < 1$, $K_2 \prec R_{t_i}$, and $0 \prec K_3 \prec \frac{\tau_\theta}{\beta L_{t_i}}(R_{t_i} - K_2)(1 - K_1)$.

In general, the smaller values of $\tau_v > 0$, $\tau_\theta > 0$, and $\tau_\phi > 0$ improve the speed of responses in voltage and current trajectories of dc–dc converters. Moreover, as one can observe from the control design algorithm, the exact value of R_{t_i} and L_{t_i} are not required for the controller design as the upper bound of K_2 and K_3 depends on these two parameters. In general, K_2 can be chosen as a negative value regardless of R_{t_i}. Furthermore, the value of K_3 plays a tradeoff between the rise time and

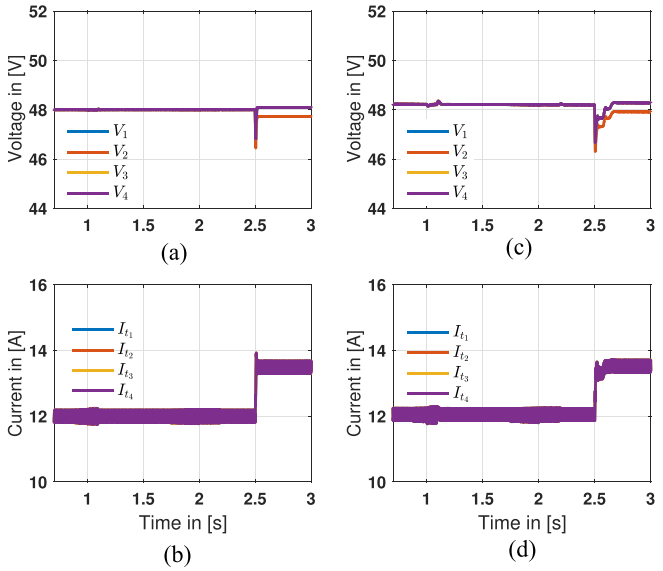

Fig. 3. Comparison between the proposed secondary control strategy in (9)–(11) and the conventional secondary control in (8). (a), (b) Voltage and current trajectories of converters using the proposed secondary control strategy in this article. (c), (d) Voltage and current trajectories of converters using the distributed secondary control strategy in [9].

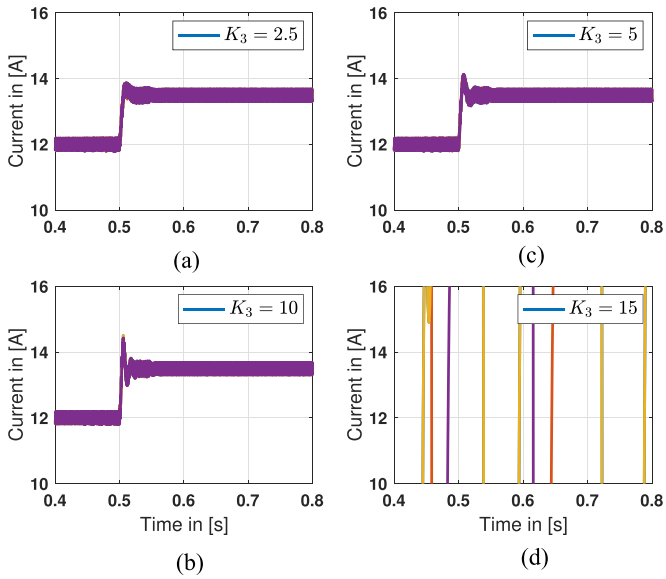

Fig. 4. Impact of the control parameter K_3 on the current trajectories of DG units.

overshoot in the voltage and current profiles of dc microgrids, i.e., the larger K_3, the faster voltage and current responses with larger overshoot. Note that the term $K_P(\theta(t) - I_t(t))$ in the proposed secondary controller is (10) and improves the dynamics responses of microgrids by preventing the occurrence of oscillations.

V. Results

In this section, the performance of the proposed distributed control scheme in (9)–(11) is evaluated using experimental results and compared with a recent existing distributed controller in [9] by means of a simulation case study.

A. Simulation Results

In this section, the performance of the proposed distributed control framework is compared with the proposed secondary control approach in [9] presented in (8). To this end, a dc microgrid with $n = 4$ dc–dc converters and $m = 5$ lines whose topology is shown in Fig. 2 is utilized. The parameters of the microgrid and its distributed controller are given in Appendix C. The parameters of the distributed secondary controller in (8) are designed as $c_i = 10$ and $\gamma_i = 2$, $i = 1, \ldots, 4$. Moreover, it is assumed that $I_1^{\text{rated}} = \cdots = I_4^{\text{rated}}$.

Case study (i)—Comparison: Fig. 3 compares the performance of both distributed control strategies with respect to disconnection of line 2 at $t = 1$ s, the reconnection of line 2 at $t = 1.75$ s, and a load change at PCC 2 at $t = 2.5$ s. As discussed in Example 1, the proposed distributed control strategy in (9)–(11) requires fewer communication links compared with (8). Furthermore, the results in Fig. 3 show that the proposed distributed controller in (9)–(11) provides faster and more smooth responses compared with the distributed secondary controller in [9].

Case study (ii)—Impact of the control parameters on performance: As discussed in Section IV-C, K_3 impacts the transient behavior of dc microgrids, i.e., increasing the value of K_3 increases the overshoot in the current trajectories of DG units. Moreover, the stability analysis in Section III shows that K_3 must be upper bounded for the stability of microgrids. In this case study, the impact of K_3 on the stability and performance of the microgrid is demonstrated. To this end, the value of K_3 is chosen to be 2.5, 5, 10, and 15. The performance of the microgrid with the different values of K_3 is evaluated under a load change at $t = 0.5$ s. The current and voltage trajectories of DG units are, respectively, shown in Figs. 4 and 5. As one can observe from these two figures, by increasing the value of K_3 to 15, the microgrid becomes unstable. The results of this case study confirm the theoretical results presented in Theorem 1. Moreover, they highlight that while the proposed secondary controller relies on fewer communication requirements (less exchanged data amongst DG units' controllers), it provides satisfactory performance in terms of voltage balancing and current sharing.

B. Experimental Results

We consider an experimental setup of a dc microgrid with $n = 3$ dc–dc buck converters connecting in a loop topology with $m = 3$ lines. The experimental setup is shown in Fig. 6. The electrical and control parameters of the dc microgrid under study are given in Appendix D. The communication graph in the distributed control layer is based on the following (oriented) incidence matrix:

$$\mathbb{B} = \begin{bmatrix} 1 & 0 & 1 \\ -1 & 1 & 0 \\ 0 & -1 & -1 \end{bmatrix}. \tag{23}$$

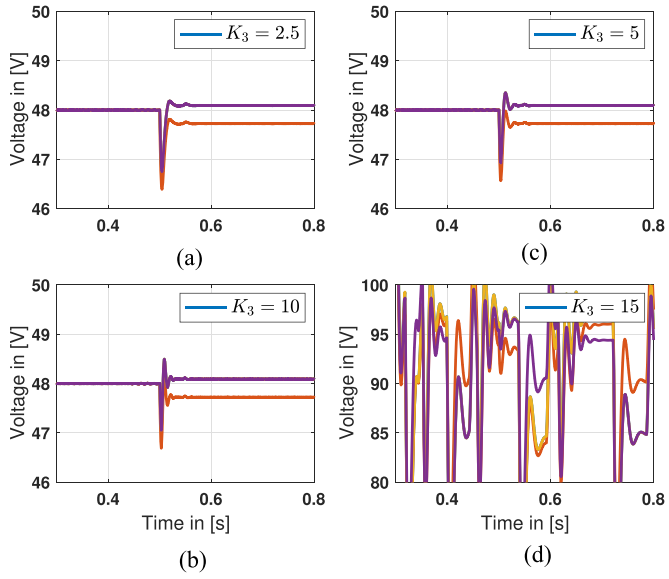

Fig. 5. Impact of the control parameter K_3 on the voltage trajectories of DG units.

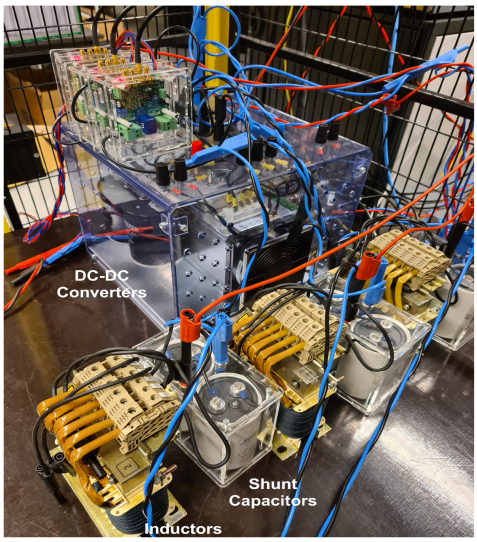

Fig. 6. Experimental setup of a dc microgrid consisting of $n = 3$ DG units.

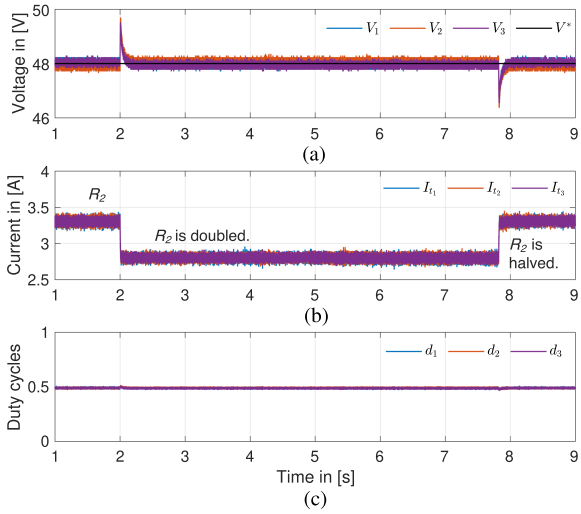

Fig. 7. Equal current sharing and voltage balancing against load changes. (a) PCC voltage trajectories. (b) Current signals of converters. (c) Duty cycles of converters.

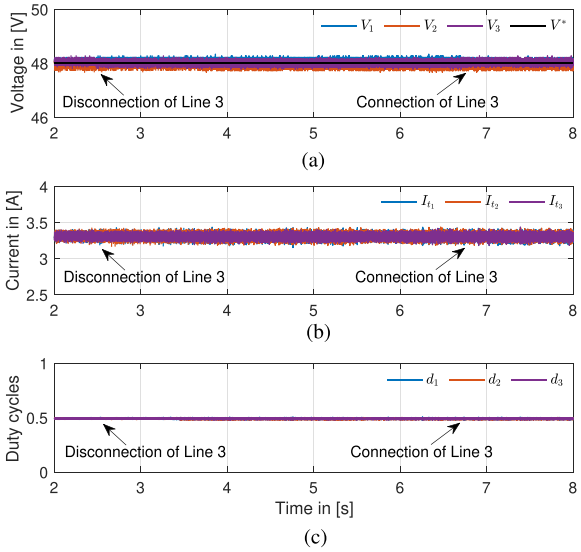

Fig. 8. Equal current sharing and voltage balancing against line disconnection and connection. (a) PCC voltage trajectories. (b) Current signals of converters. (c) Duty cycles of converters.

C. Voltage Balancing and Equal Current Sharing

In order to evaluate the performance of the proposed control strategy in voltage balancing and equal current sharing, it is assumed that all dc–dc converters have equal generation capacities, i.e., $I_1^{\text{rated}} = I_2^{\text{rated}} = I_3^{\text{rated}}$. The performance of the proposed distributed control strategy in (9)–(11) is verified under several case studies, such as voltage tracking, robustness to load changes, and topology changes in microgrids.

Case study (i)—Robustness to load changes: The second case study illustrates the robustness feature of the proposed control strategy with respect to load changes. To this end, it is assumed that the load resistance at PCC 2 (R_2) is doubled at $t = 2$ s and then halved at $t = 7.8$ s. In this case study, the voltage reference V^* is set at 48 V. Fig. 7 shows the voltage and current trajectories as well as the duty cycles of converters. As one can observe from Fig. 7, the voltage balancing and balanced current sharing objectives are achieved regardless of uncertainties in the load parameters.

Case study (ii)—Robustness to microgrid topology changes: In this case study, we assume that line 3 connecting DG 1 to DG 3 is disconnected at $t = 2.5$ s due to faults and reconnected at $t = 6.7$ s. As a result of this line disconnection, the topology of the dc microgrid changes. The dynamic responses of DG units are shown in Fig. 8. The results in Fig. 8 reveal the robust performance of the proposed distributed control approach to uncertainties in the topology of dc microgrids.

Note that the proposed distributed controller regulates the PCC voltages to be close to $V^* = 48$ V; however, they are

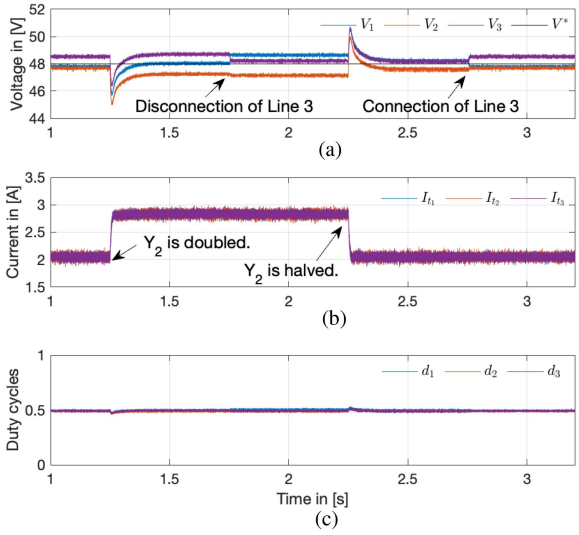

Fig. 9. Impacts of power lines with different resistance values on equal current sharing and voltage balancing. (a) PCC voltage trajectories. (b) Current signals of converters. (c) Duty cycles of converters.

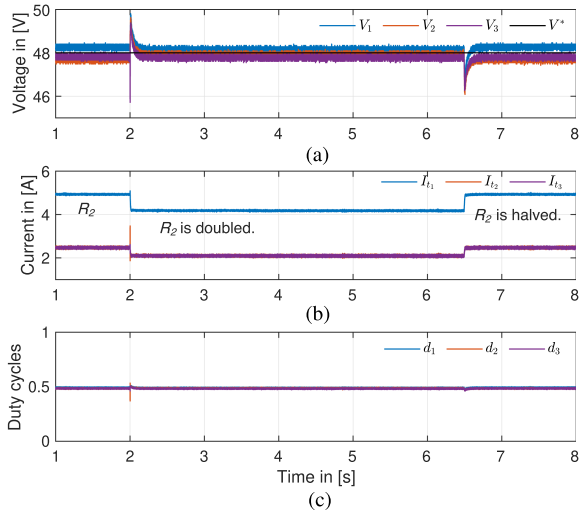

Fig. 10. Proproportional current sharing and voltage balancing against load changes. (a) PCC voltage trajectories. (b) Current signals of converters. (c) Duty cycles of converters.

not exactly equal to V^*, as this violates the current-sharing requirement.

Case study (iii)—Performance evaluation under different line parameters: In order to evaluate the performance of the proposed secondary controller for the microgrid with different line parameters, it is assumed that the lines have different resistance values ($R_1 = 1\ \Omega$, $R_2 = 0.5\ \Omega$, and $R_3 = 0.25\ \Omega$). It is assumed that the load conductance at PCC 2 is doubled and halved at $t = 1.25$ s and $t = 2.25$ s, respectively. Moreover, Line 3 connecting DG 1 and DG 3 is disconnected and reconnected at $t = 1.75$ s and $t = 2.75$ s. The results of this case study, which are shown in Fig. 9, demonstrate that the deviation of the PCC voltages from the nominal voltage V^* is slightly larger than the previous case (i.e., line parameters are equal), but they are still within the accepted range of $\pm 10\%$ of V^*. Moreover, the results confirm the steady-state value of PCC voltages $\bar{V}$ given in (15).

D. Voltage Balancing and Proportional Current Sharing

Case study (iv)—Robustness to load variation and microgrid topology changes: In the fourth case study, it is assumed that DG 1's generation capacity is twice of DG 2 and DG 3, i.e., $I_1^{\text{rated}} = 2I_2^{\text{rated}} = 2I_3^{\text{rated}}$. As a result, total load demand should proportionally be shared amongst DG units. Figs. 10 and 11 show the proportional current sharing and voltage balancing capabilities of the proposed control strategy against voltage reference changes, load changes, and line disconnection. The changes in load conditions and line failure are the same as the ones in the case studies (i) and (ii). As the voltage and current trajectories are shown in Figs. 10 and 11, the proposed distributed control strategy in (9)–(11) guarantees voltage balancing and proportional current sharing with respect of different sources of uncertainties in dc microgrids, e.g., load uncertainty and changes in the topology of dc microgrids.

Case study (v)—Robustness to dc voltage variations at the input side of converters: In the final experimental case study,

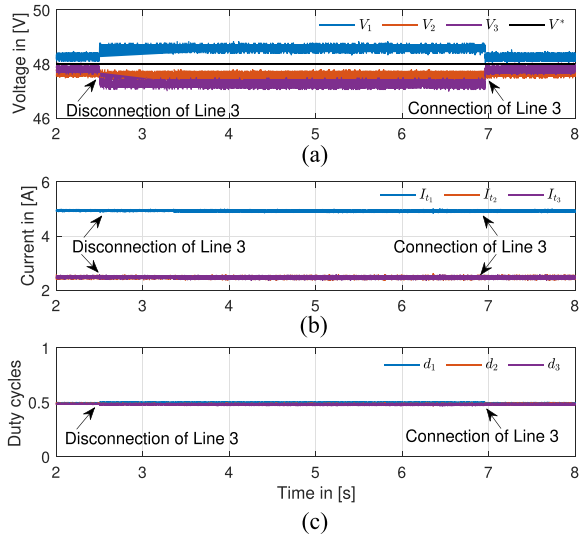

Fig. 11. Proproportional current sharing and voltage balancing against line disconnection and connection. (a) PCC voltage trajectories. (b) Current signals of converters. (c) Duty cycles of converters.

we test the performance of the proposed distributed controller against variations in dc voltages at the input side of the converters. To this purpose, $V_{dc,i}$, $i = 1, 2, 3$, is stepped up to 110 V, then stepped down to 90 V, and finally stepped up to 100 V. The voltage and current trajectories of the dc microgrid, as well as the duty cycles of the converters are shown in Fig. 12. As Fig. 12(c) shows, upon changing $V_{dc,i}$, the control inputs ($d_i(t)$) make an immediate action so that voltage balancing and current sharing are ensured. As a result, by changing the input voltage of converters, their output voltage remains unchanged.

Case study (vi)—Performance evaluation under different line parameters: The case study (iii) is repeated for the case of proportional current sharing. Fig. 13 shows the results of this case study. Although the voltage deviation from V^* is slightly higher than the case of equal line parameters, the results are

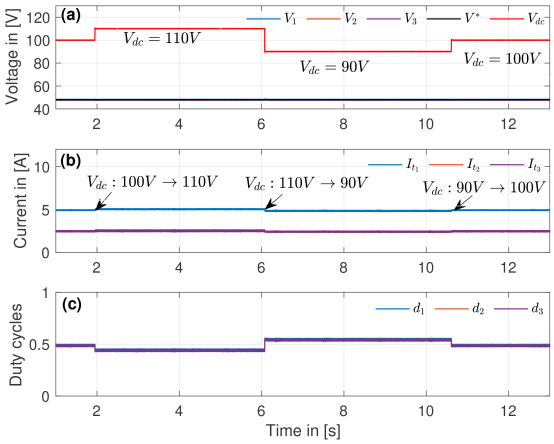

Fig. 12. Proportional current sharing and voltage balancing against variations in the dc voltages at the input side of converters. (a) Input and output voltage of converters. (b) Current signals of converters. (c) Duty cycles of converters.

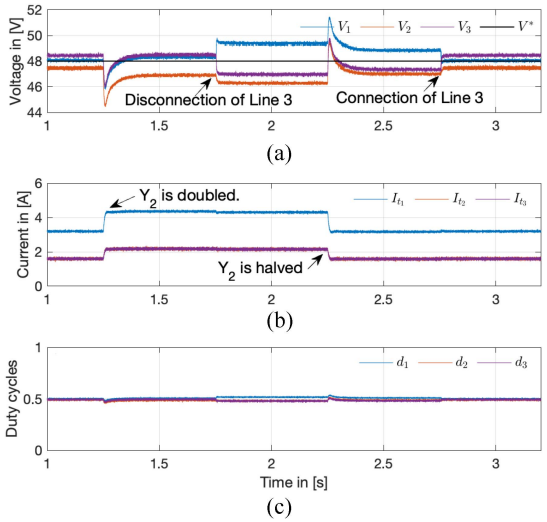

Fig. 13. Impacts of power lines with different resistance values on proportional current sharing and voltage balancing. (a) PCC voltage trajectories. (b) Current signals of converters. (c) Duty cycles of converters.

satisfactory (the voltage deviation from V^* is within the accepted range of $\pm 10\%$ of V^*). Moreover, the results demonstrate that the current sharing objective is ensured even in the case of unequal line parameters.

E. DC Microgrids with Radial Topologies

To show that our proposed secondary control approach is applicable to dc microgrids under flexible and different topologies, we consider the experimental setup of a dc microgrid with $n = 3$ DG units connecting via radial structure. In this microgrid topology, DG 1 is connected to both DG 2 and DG 3 via Line 1 with the resistance $R_1 = 1\ \Omega$ and Line 2 with the resistance $R_2 = 0.25\ \Omega$. DG 2 and DG 3 are not connected via any lines.

Case Study (vii): The performance of the radial microgrid is evaluated against load variation under following two scenarios:

1) the current capacity of DG units is equal and

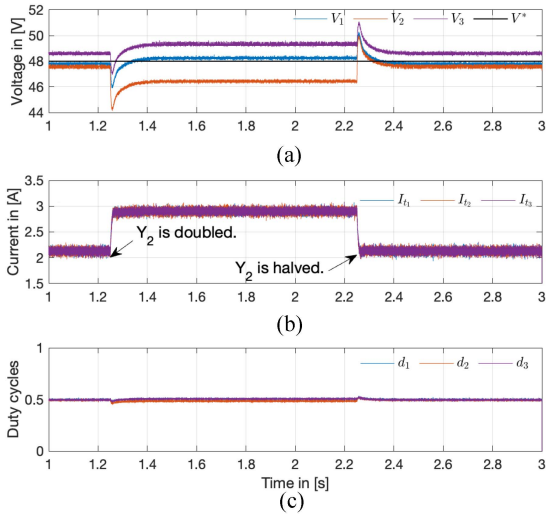

Fig. 14. Equal current sharing and voltage balancing for the microgrid with the radial topology. (a) PCC voltage trajectories. (b) Current signals of converters. (c) Duty cycles of converters.

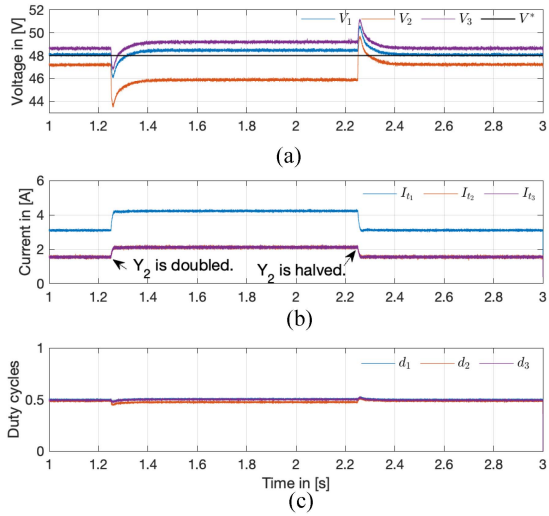

Fig. 15. Proportional current sharing and voltage balancing for the microgrid with the radial topology. (a) PCC voltage trajectories. (b) Current signals of converters. (c) Duty cycles of converters.

2) DG 1's generation capacity is twice of the capacity of DG 2 and DG 3.

The results of this case study for both scenarios are shown in Figs. 14 and 15, respectively. As one can observe from the figures, the current-sharing and voltage balancing objectives are ensured; furthermore, $|\bar{V}_i - V^*| \leq 0.1V^*; i = 1, 2, 3$.

VI. Conclusion

In this article, a novel sparsity-promoting consensus-based distributed secondary control scheme in terms of exchanged data for dc microgrids is proposed. The proposed robust distributed secondary control algorithm ensures voltage balancing and current-sharing requirements in dc microgrids. The stability of dc microgrids with the proposed control approach is analyzed

based on the Lyapunov theory and LaSalle's invariance principle. Building on this analysis, the sufficient stability conditions for the stability of dc microgrids are derived. The effectiveness of the proposed control approach is verified via simulation and experimental case studies. The robustness and resilience analysis of the proposed secondary control approach with respect to communication delay, packet loss, and cyber-attacks will be considered as the future scope of this work.

APPENDIX A

For an undirected weighted graph $\mathcal{G} = (\mathcal{V}, \mathcal{E})$ of order n and with m edges, the incidence matrix $\mathbb{B} \in \mathbb{R}^{n\times m}$ has specific properties as stated in the following lemma.

Lemma 2: The (oriented) incidence matrix $\mathbb{B} \in \mathbb{R}^{n\times m}$ of a connected undirected graph $\mathcal{G}$ of n nodes and m edges has the following properties.

1) $\text{rank}(\mathbb{B}) = n - 1$.
2) $\mathbb{B}^T\mathbf{1}_n = 0$ ($\mathbf{1}_n^T\mathbb{B} = 0$).
3) $\mathbb{B}\mathbb{B}^+ = \mathbf{I}_n - \frac{1}{n}\mathbf{1}_n\mathbf{1}_n^T$.
4) $\mathbb{B}\mathbb{B}^+\mathbb{B} = \mathbb{B}$.
5) $\mathbb{B}^+\mathbf{1}_n = 0$.
6) $\mathbb{B}x = 0 \Leftrightarrow x^T\mathbb{B}^+ = 0$.

Here, $\mathbb{B}^+ \in \mathbb{R}^{m\times n}$ is the Moore–Penrose generalized inverse of $\mathbb{B}$.

Proof: See [15] and [20]. □

APPENDIX B
PROOF OF LEMMA 1

Proof: The equilibria of (13) satisfy the following algebraic equations:

$$-K\mathbb{B}^T W^{-1}\bar{I}_t = 0 \tag{24a}$$

$$-\beta(\bar{V} - \mathbf{1}_n V^*) + K_P(\bar{\theta} - \bar{I}_t) + KW^{-1}\mathbb{B}\bar{v} = 0 \tag{24b}$$

$$\bar{\theta} - \bar{I}_t = 0 \tag{24c}$$

$$\bar{I}_t - \mathbb{B}_e\bar{I} - [Y]\,\bar{V} = 0 \tag{24d}$$

$$\mathbb{B}_e^T\bar{V} - [R]\,\bar{I} = 0 \tag{24e}$$

where $(\bar{I}_t, \bar{V}, \bar{v}, \bar{\theta}, \bar{I})$ are the steady-state value of (I_t, V, v, θ, I). Due to the properties of incidences matrix (see Lemma 2), from (24a) and (24d), one obtains that $\bar{I}_t = W\mathbf{1}_n i^*$, where $i^* = (\mathbf{1}_n^T W\mathbf{1}_n)^{-1}\mathbf{1}_n^T[Y]\bar{V}$. Moreover, from (24c), one obtains that $\bar{\theta} = \bar{I}_t$. Replacing $\bar{I}_t$ with $\bar{\theta}$ in (24b) leads to the following equation:

$$-\beta(\bar{V} - \mathbf{1}_n V^*) + KW^{-1}\mathbb{B}\bar{v} = 0. \tag{25}$$

By left multiplying of both sides of the abovementioned equation by $\mathbf{1}_n^T W$ and invoking the properties of the incidence matrix $\mathbb{B}$, one obtains that

$$-\beta\mathbf{1}_n^T W(\bar{V} - \mathbf{1}_n V^*) = 0. \tag{26}$$

Since $\beta \neq 0$, it follows that $\mathbf{1}_n^T W\bar{V} = \mathbf{1}_n^T W\mathbf{1}_n V^*$.

Premultiplying both sides of (25) by $K^{-1}\mathbb{B}\mathbb{B}^+W$, where $\mathbb{B}^+$ is the generalized inverse of $\mathbb{B}$, results in the following equation:

$$\begin{aligned}\beta K^{-1}\mathbb{B}\mathbb{B}^+W(\bar{V} - \mathbf{1}_n V^*) &= \mathbb{B}\mathbb{B}^+\mathbb{B}\bar{v} \\ &= \mathbb{B}\bar{v}.\end{aligned} \tag{27}$$

Note that $\mathbb{B}\mathbb{B}^+\mathbb{B} = \mathbb{B}$ (see Property 4 in Lemma 2). As a result

$$\begin{aligned}&\mathbb{B}\left(\bar{v} - \beta K^{-1}\mathbb{B}^+W(\bar{V} - \mathbf{1}_n V^*)\right) = 0. \\ &\Rightarrow \bar{v} = \alpha v_0 + \beta K^{-1}\mathbb{B}^+W(\bar{V} - \mathbf{1}_n V^*).\end{aligned} \tag{28}$$

where $v_0 \in \ker(\mathbb{B})$ and $\alpha \in \mathbb{R}$ are constants. According to (14), $v_0^T\bar{v} = v_0^T v(0)$; therefore, $\bar{v}$ is rewritten as follows:

$$\bar{v} = \begin{cases} \left(\frac{v_0^T v(0)}{v_0^T v_0}\right) v_0 + \beta K^{-1}\mathbb{B}^+W(\bar{V} - \mathbf{1}_n V^*) & \text{if } v_0 \neq 0 \\ \beta K^{-1}\mathbb{B}^+W(\bar{V} - \mathbf{1}_n V^*) & \text{if } v_0 = 0. \end{cases} \tag{29}$$

To obtain the abovementioned equation, we use that $v_0^T\mathbb{B}^+ = 0$ (see Property 6 in Lemma 2). From (24e) and (24d), one obtains that $\bar{I} = [R]^{-1}\mathbb{B}_e^T\bar{V}$ and $\bar{I}_t = \mathbb{B}_e[R]^{-1}\mathbb{B}_e^T\bar{V} + [Y]\bar{V}$. Hence,

$$\left((\mathbf{1}_n^T W\mathbf{1}_n)^{-1}W\mathbf{1}_n\mathbf{1}_n^T\right)[Y]\,\bar{V} = \mathbb{L}_e\bar{V} + [Y]\,\bar{V}. \tag{30}$$

where $\mathbb{L}_e = \mathbb{B}_e[R]^{-1}\mathbb{B}_e^T$ represents the Laplacian matrix of the electrical circuit of the dc microgrid. The abovementioned equation can be rewritten as

$$\mathbb{L}_t\bar{V} + \mathbb{L}_e\bar{V} = 0 \tag{31}$$

where $\mathbb{L}_t = (\mathbf{I}_n - (\mathbf{1}_n^T W\mathbf{1}_n)^{-1}W\mathbf{1}_n\mathbf{1}_n^T)[Y]$. Taking into account (26) and (31), $\bar{V}$ can be obtained from the following equation:

$$\begin{bmatrix} \mathbb{L}_t + \mathbb{L}_e \\ \mathbf{1}_n^T W \end{bmatrix}\bar{V} = \begin{bmatrix} 0 \\ \mathbf{1}_n^T W\mathbf{1}_n V^* \end{bmatrix}. \tag{32}$$

This completes the proof. □

APPENDIX C
PARAMETERS OF THE SIMULATED DC MICROGRID

The dc microgrid in Fig. 2 consists of $n = 4$ dc–dc buck converters connecting via $m = 5$ distribution lines and equipped with a distributed controller whose structure is given in (9)–(11).

DC–DC converters: $V_{\text{dc},i} = 100$ V, $L_{t_i} = 2.64$ mH, $C_{t_i} = 1.1$ mF, and $Y_i = 0.25\ \Omega^{-1}$; $i = 1, 2, 3, 4$. The switching frequency is $f_{\text{sw}} = 30$ kHz.

Lines: $R_1 = \cdots = R_4 = 0.25\ \Omega$, $R_5 = 0.75\ \Omega$, and $L_k = 2$ μH; $k = 1, \ldots, 5$.

Controllers: $\tau_v = 0.005, \tau_\theta = 0.1, \tau_\phi = 0.005, \beta = 20, K = 1$, $K_P = 2.5$, $K_1 = -1$, $K_2 = -3$, and $K_3 = 2.5$.

APPENDIX D
PARAMETERS OF THE EXPERIMENTAL SETUP

The dc microgrid in the experimental setup in Fig. 6 consists of $n = 3$ dc–dc buck converters connecting via $m = 3$ distribution lines and equipped with a distributed controller whose structure is given in (9)–(11).

DC–DC converters: $V_{\text{dc},i} = 100$ V, $L_{t_i} = 1.72$ mH, $C_{t_i} = 1.1$ mF, and $Y_i = \frac{1}{15}\ \Omega^{-1}$; $i = 1, 2, 3$. The switching frequency is $f_{\text{sw}} = 20$ kHz.

Lines: $R_i = 0.5\ \Omega$; $i = 1, 2, 3$.

Controllers: $\tau_v = 0.005, \tau_\theta = 0.1, \tau_\phi = 0.005, \beta = 20, K = 1$, $K_P = 2.5$, $K_1 = -1$, $K_2 = -3$, and $K_3 = 2.5$.

REFERENCES

[1] G. Strbac, N. Hatziargyriou, J. P. Lopes, C. Moreira, A. Dimeas, and D. Papadaskalopoulos, "Microgrids: Enhancing the resilience of the european megagrid," *IEEE Power Energy Mag.*, vol. 13, no. 3, pp. 35–43, May/Jun. 2015.

[2] T. Dragicevic, X. Lu, J. C. Vasquez, and J. M. Guerrero, "DC microgrids–Part II: A. review of power architectures, applications, and standardization issues," *IEEE Trans. Power Electron.*, vol. 31, no. 5, pp. 3528–3549, May 2016.

[3] V. Nasirian, S. Moayedi, A. Davoudi, and F. L. Lewis, "Distributed cooperative control of dc microrgids," *IEEE Trans. Power Electron.*, vol. 30, no. 4, pp. 2288–2303, Apr. 2015.

[4] S. Moayedi, V. Nasirian, F. L. Lewis, and A. Davoudi, "Team-oriented load sharing in parallel dc–dc converters," *IEEE Trans. Ind. Appl.*, vol. 51, no. 1, pp. 479–490, Jan./Feb. 2015.

[5] J. Zhao and F. Dorfler, "Distributed control and optimization in dc microgrids," *Automatica*, vol. 61, pp. 18–26, Nov. 2015.

[6] Z. Liu, M. Su, Y. Sun, H. Han, X. Hou, and J. M. Guerrero, "Stability analysis of dc microgrids with constant power load under distributed control methods," *Automatica*, vol. 90, pp. 62–72, 2018.

[7] B. Fan, S. Guo, J. Peng, Q. Yang, W. Liu, and L. Liu, "A consensus-based algorithm for power sharing and voltage regulation in dc microgrids," *IEEE Trans. Ind. Informat.*, vol. 16, no. 6, pp. 3987–3996, Jun. 2020.

[8] B. Fan, J. Peng, Q. Yang, and W. Liu, "Distributed periodic event-triggered algorithm for current sharing and voltage regulation in dc microgrids," *IEEE Trans. Smart Grid*, vol. 11, no. 1, pp. 577–589, Jan. 2020.

[9] S. Zuo, T. Altun, F. L. Lewis, and A. Davoudi, "Distributed resilient secondary control of dc microgrids against unbounded attacks," *IEEE Trans. Smart Grid*, vol. 11, no. 5, pp. 3850–3859, Sep. 2020.

[10] M. S. Sadabadi, "A distributed control strategy for parallel dc–dc converters," *IEEE Contr. Syst. Lett.*, vol. 5, no. 4, pp. 1231–1236, Oct. 2021.

[11] M. S. Sadabadi, S. Sahoo, and F. Blaabjerg, "Stability-oriented design of cyberattack-resilient controllers for cooperative dc microgrids," *IEEE Trans. Power Electron.*, vol. 37, no. 2, pp. 1310–1321, Feb. 2022.

[12] S. Sahoo and S. Mishra, "An adaptive event-triggered communication-based distributed secondary control for dc microgrids," *IEEE Trans. Smart Grid*, vol. 9, no. 6, pp. 6674–6683, Nov. 2018.

[13] S. A. Alavi, K. Mehran, Y. Hao, A. Rahimian, H. Mirsaeedi, and V. Vahidinasab, "A distributed event-triggered control strategy for dc microgrids based on publish-subscribe model over industrial wireless sensor networks," *IEEE Trans. Smart Grid*, vol. 10, no. 4, pp. 4323–4337, Jul. 2019.

[14] J. Peng, B. Fan, Q. Yang, and W. Liu, "Distributed event-triggered control of dc microgrids," *IEEE Syst. J.*, vol. 15, no. 2, pp. 2504–2514, Jun. 2021.

[15] F. Bullo, "Lectures on network systems, 1.6 ed. kindle direct publishing," 2022. [Online]. Available: http://motion.me.ucsb.edu/book-lns

[16] M. S. Sadabadi, "Line-independent plug-and-play voltage stabilization and L_2 gain performance of dc microgrids," *IEEE Contr. Syst. Lett.*, vol. 5, no. 5, pp. 1609–1614, Nov. 2021.

[17] F. Dorfler and F. Bullo, "Kron reduction of graphs with application to electrical networks," *IEEE Trans. Circuits Syst. I Regular Papers*, vol. 60, no. 1, pp. 150–163, Jan. 2013.

[18] M. Cucuzzella et al., "A robust consensus algorithm for current sharing and voltage regulation in dc microgrids," *IEEE Trans. Control Syst. Technol.*, vol. 27, no. 4, pp. 1583–1595, Jul. 2019.

[19] H. K. Khalil, *Nonlinear Systems*. Upper Saddle River, NJ, USA: Prentice Hall, 2006.

[20] Y. Ijiri, "On the generalized inverse of an incidence matrix," *J. Soc. Ind. Appl. Math.*, vol. 13, no. 3, pp. 827–836, Sep. 1965.